# Experimental investigation of bubble breakup in bubble chains rising in a liquid metal

Keplinger, O.; Shevchenko, N.; Eckert, S.;

Originally published:

April 2019

**International Journal of Multiphase Flow 116(2019), 39-50**

DOI: https://doi.org/10.1016/j.ijmultiphaseflow.2019.03.027

Perma-Link to Publication Repository of HZDR:

https://www.hzdr.de/publications/Publ-28079

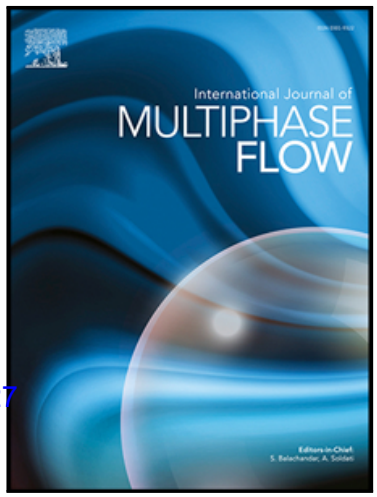


# Experimental investigation of bubble breakup in bubble chains rising in a liquid metal

O. Keplinger , N. Shevchenko , S. Eckert

PII: S0301-9322(18)30698-0
DOI: https://doi.org/10.1016/j.ijmultiphaseflow.2019.03.027
Reference: IJMF 3003

To appear in: *International Journal of Multiphase Flow*

Received date: 28 September 2018
Revised date: 19 February 2019
Accepted date: 29 March 2019

Please cite this article as: O. Keplinger , N. Shevchenko , S. Eckert , Experimental investigation of bubble breakup in bubble chains rising in a liquid metal, *International Journal of Multiphase Flow* (2019), doi: https://doi.org/10.1016/j.ijmultiphaseflow.2019.03.027

Highlights

- X-ray radiography combined with high-speed video imaging was used to visualize the bubble breakup in bubble chains rising in opaque liquid metals. The processes of bubble breakup were found to proceed in a qualitatively similar way as for the case of water or highly viscous fluids. The observations indicate that the turbulent flow in the immediate vicinity of the bubbles has an important influence on whether breakup occurs or not.

# Experimental investigation of bubble breakup in bubble chains rising in a liquid metal

O. Keplinger, N. Shevchenko, S. Eckert.

Helmholtz-Zentrum Dresden-Rossendorf
Bautzner Landstraße 400
01328 Dresden
Germany

Corresponding author: E-mail: o.keplinger@hzdr.de

**Abstract**

The process of bubble breakup in a liquid metal was studied by X-ray radiography and high-speed video imaging. Argon gas bubbles were injected through a single orifice at the bottom of a rectangular vessel filled with the eutectic GaInSn alloy. Moderate gas flow rates were applied at isothermal conditions resulting in the formation of bubble chains. The bubble breakup events observed in the chosen experimental geometry were mainly initiated by bubble collisions or by the effect of local shear flow. We present experimental results accompanied by statistical analysis of the bubble breakup frequency, number of daughter bubbles and their size distribution, bubble velocities before and after the breakup process for a broad range of Argon gas flow rates.

**Key words:** Liquid metal; Two-phase flow; Bubble chain; Bubble breakup; X-ray radiography.

## Introduction

Liquid metal two-phase flows are frequently used for technological processes in metallurgy and metal casting. For example, Argon gas is injected during the secondary-metallurgical treatment of liquid steel to improve the melt cleanliness by the flotation process. During flotation the Argon gas bubbles separate undesired inclusions from the melt by the following mechanisms: (i) evocation of particle agglomeration by the shear flow in the bubble wake, (ii) capturing the particles at the gas-liquid interface, and (iii) transporting them towards the slag layer at the free surface. This separation process is highly dependent on both the properties of the inclusions and the bubble size distribution which defines the interfacial area within the melt. The interfacial area itself determines the interfacial mass, momentum and energy exchange and is strongly modified by bubble coalescence and breakup. For example, bubble-bubble and bubble-flow interactions which lead to breakup increase the number of bubbles, decrease the mean bubble size and, therefore, increase the gas-liquid interfacial area. Fundamental analysis indicated that the use of smaller bubbles is the most effective approach to increase the probability of collision with particles inside the melt and to reduce the probability of their detachment from bubbles (Tao, 2005). As a consequence, bubble breakup is supposed to enhance the efficiency of flotation processes. Therefore, different measures

such as impellers are used in industrial applications for inducing bubble breakup (Martín et al., 2008; Takahashi et al., 1992).

Previous works focus mainly on viscous, inertial or complex turbulent breakup of single bubbles in transparent liquids (Chen et al., 2005; Lee et al., 1987a; Lehr et al., 2002; Luo and Svendsen, 1996; Martínez-Bazán et al., 1999a, 1999b; Qian et al., 2006; Wang et al., 2003). Such phenomena are governed by complex underlying physics which gets even more complicated when bubble-bubble interaction is involved. Nevertheless, even a complete understanding of single bubble breakup is not yet available.

The rise of a multitude of bubbles in form of a chain or a plume inside a low-viscosity liquid pool produces a turbulent flow in the fluid. As a result bubble breakup can be initiated by several reasons: turbulent fluctuations, interaction and collision with turbulent eddies or other bubbles, viscous shear stress, shearing-off processes and due to interfacial perturbations caused by the Rayleigh-Taylor (Clift et al., 1978; Fan and Tsuchiya, 1990) and the Kelvin-Helmholtz (Kitscha and Kocamustafaogullari, 1989) instability. In general, the bubbles initially undergo a deformation caused by pressure fluctuations along the bubble surface or by collisions with turbulent eddies (Liao and Lucas, 2009a). When the balance between dynamic pressure around the bubble and its surface tension is violated the bubble starts to deform and stretch leading to indentation, necking and pinching. The breakup in this case is often governed by the turbulent kinetic energy of the bubble (Chatzi and Lee, 1987; Chatzi et al., 1989; Coulaloglou and Tavlarides, 1977) or by the turbulent kinetic energy of the hitting eddy (Lee et al., 1987a, 1987b; Luo and Svendsen, 1996; Martínez-Bazán et al., 1999a, 1999b; Prince and Blanch, 1990; Tsouris and Tavlarides, 1994). Alopaeus et al. (2002) and Narsimhan et al. (1984) considered the influence of velocity fluctuations occurring around the bubble. Lehr et al. (2002) compared the inertial force of the hitting eddy and the interfacial force of the smallest daughter fragment. Some studies combine several of these criteria (Wang et al., 2003; Zhao and Ge, 2007). In case of a breakage due to viscous shear forces, the bubble undergoes deformation due to the velocity gradient across the interface of the bubble. The breakage then appears when the surface tension is no longer able to maintain the bubble shape (Kocamustafaogullari and Ishii, 1995; Renardy et al., 2002; Renardy and Cristini, 2001a, 2001b). The shear-off process is observed for large bubbles moving in highly viscous flows (e.g. slug bubbles). In case when the relative velocity is high enough the balance between the viscous shear force and the surface tension at skirt of the slug bubble is disturbed and the bubble skirt becomes unstable and sheds from the bubble accompanied by the generation of a large number of small bubbles at the rim (Liao and Lucas, 2009a). For low viscosity liquids (for example for air-water system) this effect is caused by the gas velocity profile inside the bubble cap which moves at the terminal velocity. There is a distinct velocity gradient across the gas-liquid interface which is responsible for the penetration of the gas into the liquid boundary layer where it forms small bubbles (Fu and Ishii, 2003; Liao et al., 2015; Liao and Lucas, 2009b; Suhas S. Jain, 2017). It is hardly to be expected that such an effect also occurs in liquid metals, since their surface tension is significantly higher than in aqueous systems.

The appearance of bubble breakage in most cases can be quantified by their deformation degree or by the Weber number (Liao et al., 2015; Liao and Lucas, 2009b):

$$We = \frac{\rho u^2 d}{\sigma}, \tag{1}$$

where $\rho$ is the liquid density, $u$ is the liquid velocity, $d$ is the bubble diameter and $\sigma$ is the surface tension. Risso and Fabre ( 1998) showed that for air bubbles in tap water a minimum $We$ number of about 5 is necessary for breakup when turbulence is the only reason for deformation. Also, the breakup probability is strongly correlated with the deformation experienced by the bubble: no breakup is observed for $A^*<1.5$, 75% for $1.5<A^*<2$, 100% for $A^*>2$. The maximum deformation is calculated as

$$A^* = \frac{4A_B}{\pi d_B^2}, \quad (2)$$

where $A_B$ is the bubble projection area and $d_B$ is the bubble diameter calculated from the same projection area $A_B$ assuming that the bubble is spherical. The number of daughter bubbles depends on the specific shape of the bubble during the deformation process and varies in a wide range, while the daughter size distribution is controlled by the daughter number (Ravelet et al., 2011; Risso and Fabre, 1998; Solsvik and Jakobsen, 2015a, 2015b; Vejražka et al., 2017). Hesketh et al. (1991) have observed that bubbles are more likely to breakup into unequally sized fragments. Andersson and Andersson (2006) explained the formation of unequally sized daughters by an internal flow redistribution mechanism.

It is important to note that, despite qualitative similarities in the underlying bubble interaction phenomena (Keplinger et al., 2018), the behavior of bubbles in water and in GaInSn is likely to vary significantly with respect to shape deformation due to significant differences in density and surface tension. As a consequence, the deformation of bubbles right up to breakage in a liquid metal can significantly distinguish from the observations in water. Therefore, direct investigations of bubble breakup in liquid metals become crucial.

Measurements of gas bubbles in liquid metals are generally more difficult to achieve than in water experiments because the opacity of the metals does not allow the use of powerful optical methods. So far, there are only very few experimental studies on the dynamics of bubble motion in liquid metals. Local conductivity probes (Eckert et al., 2000a, 2000b; Iguchi et al., 1997; Manera et al., 2009; Oryall and Brimacombe, 1976; Xie et al., 1992; Xie and Oeters, 1994), ultrasound techniques (Richter et al., 2018; Timmel et al., 2010; Wang et al., 2017; Zhang et al., 2005) or inductive methods (Gundrum et al., 2016; Lyu and Karcher, 2016) can be used to detect gas bubbles in liquid metals. However, all these methods are subject to certain restrictions. For example, conductivity probes are intrusive and provide only local information. Ultrasonic methods encounter problems when the number of bubbles in the measuring volume increases with increasing gas content. Multiple echoes at the bubble interfaces can create signal artifacts causing serious difficulties in data processing. Inductive methods provide a contactless method for bubble detection in liquid metal flows, but, the reconstruction of the bubble shape is still challenging and the interpretation of the signals becomes exceedingly difficult in case of interaction of multiple bubbles. X-ray radiography based on the absorption contrast between the liquid and gas phase has proven to be an efficient method for multiphase flows (Heindel, 2011; Kastengren and Powell, 2014; Mudde, 2010; Mudde et al., 2008) and especially for bubble detection in liquid metals (Davis et al., 1978; Fröhlich et al., 2013; Iguchi et al., 1995; Keplinger et al., 2018; Richter et al., 2018; Shevchenko et al., 2013; Timmel et al., 2015; Vogt et al., 2015; Wang et al., 1999). The main limitation for this technique is the thickness of the fluid volume that can be investigated due to high X-ray absorption coefficients for liquid metals. The accuracy of the X-ray radiography technique for determining bubble parameters is discussed in detail in (Keplinger et al., 2017). Another irradiation method is the neutron radiography (Baake et al., 2017; Mishima et al., 1999; Saito et al., 2005; Sarma et al., 2015) which allows the investigation of thicker measuring volumes but at the expense of image contrast.

In the present work we study the occurrence of bubble breakup in a bubble chain rising in a liquid metal. Experiments were carried out in GaInSn, a ternary alloy that is liquid at room temperature and whose material properties are very similar to those of liquid steel (Plevachuk et al., 2014). The dynamics of the bubble rising behavior was visualized by means of X-ray radiography using high-speed video imaging. We present statistical analysis of the bubble breakup frequency, number of daughter bubbles and their size distribution, bubble velocities before and after the breakup process for a broad range of Argon gas flow rates.

**Experimental setup**

Bubble visualization experiments were carried out at the X-ray laboratory at HZDR. The scheme of the experimental setup is shown in Figure 1. A continuous divergent polychromatic X-ray beam was produced by an industrial X-ray tube (GE ISOVOLT 450KV/25-55 from GE Sensing & Inspecting Technologies GmbH) operating at a voltage of 320 kV and a current of 14 mA. The X-ray beam penetrates the liquid metal along the narrow extension of the container as shown in Figure 1. The non-absorbed part of the beam that can be estimated by the Beer-Lambert law:

$$I=I_0 e^{-\mu D}, \quad (3)$$

where $I_0$ is the primary beam intensity, $\mu$ is the X-ray attenuation coefficient and $D$ is the thickness of the liquid metal, impinges on a scintillation screen (SecureX HB from Applied Scintillation Technologies) that is attached to the outer wall of the container. The X-ray intensity is then converted into visible light in the scintillator that is further deflected by a mirror onto a sCMOS sensor plane of the high-speed video camera (pco.edge 5.5 from PCO) through a lens system (custom-made design by Thalheim-Spezial-Optik). The camera field of view (FOV) was ~60×130 mm$^2$. In the selected experiments the images were captured at a frame rate of 100 frames per second. An exposure time of 3 milliseconds results in a good signal-to-noise ratio without causing significant bubble blurring of the bubble images due to their high rising velocities.

The vessel made of acrylic glass with a rectangular cross-section of 12×144 mm$^2$ was filled with eutectic composition of the ternary GaInSn alloy (Plevachuk et al., 2014) up to 144 mm height resulting in a total aspect ratio of 1. The inert Argon gas was injected through a single long bevel stainless steel orifice with an inner diameter of 0.75 mm (from Sterican®) positioned in the middle of the cross-section just above the bottom of the vessel. Such a nozzle shape was chosen over flat orifice in order to achieve an effective damping of the bubble zig-zagging between the walls in the direction of the X-ray beam. The gas flow rate was regulated in the range from 10 to 1200 cm$^3$/min by a gas flow control system (from MKS Instruments). The experiments were conducted at room temperature and normal atmospheric pressure. Here, we would like to point out that the choice of such a fluid vessel is governed by the high X-ray attenuation coefficient of the liquid metal which restricts the dimension of the fluid vessel along the X-ray beam. The distance of 12 mm between the side walls is in the same order of magnitude as the size of the bubbles in our experiments. Therefore, the influence of the side walls on bubble characteristics (trajectory, shape and velocity) is probably not negligible especially at high gas flow rates. In general, constraining walls can cause an elongation of bubbles in the vertical direction, suppress secondary motion and alter the wake structure by reducing the wake volume and the rate of fluid circulation within the wake (Clift et al., 1978). Krishna et al. (1999) found that the side wall effect can reduce the rise velocity in water by a factor of about 0.5 at maximum. Furthermore, the authors report that the bubble rise velocity becomes independent of the bubble diameter $d_B$ for $d_B/D > 0.6$. However, Keplinger et al. (2018) have demonstrated that coalescence of two 9 mm size bubbles in GaInSn show a measurable increase of the rise velocity after the bubbles have merged.

The images were analyzed using Matlab scripts for extracting diverse parameters as bubble sizes, their trajectories and rising velocities before and after breakup. The image processing was done as follows: as a first step a shading correction is performed by dividing the image by the mean reference image measured at zero gas flow rate. Separation of individual bubbles and bubble clusters from the background is achieved by using a threshold value which was slightly above 1 (i.e. ~1.07). All pixels whose brightness is above the threshold value were assigned to the bubble area. The corresponding threshold value is derived from a calibration measurement using 5 and 10 mm diameter glass balls surrounded by GaInSn at a zero

gas flow rate and accounts X-ray scattering by the bubble surface. As a next step the images were analyzed applying the Matlab function 'regionprops' which allows to extract parameters like perimeter, area, center of mass, etc. The bubble area is converted from pixel to metric values using the scaling of the image. With the assumption of spherical bubble shapes the mean bubble diameter was calculated according to

$$d_B = 2\sqrt{A_B/\pi}, \tag{4}$$

were $A_B$ is the bubble projection area in the X-ray images. The rising velocity was calculated from the bubble trajectories according to:

$$v = \frac{l}{\Delta t}, \tag{5}$$

where $l = \sqrt{(x_2 - x_1)^2 + (y_2 - y_1)^2}$ is the distance the bubble travelled between two subsequent bubble positions during the time step $\Delta t$= 0.01s and x and y being the horizontal and vertical bubble position respectively (see Figure 2a for details). Interfaces of the bubbles which are moving in a close vicinity to each other and even overlap were defined manually. A detailed description of the image processing can be found in (Keplinger et al., 2017).

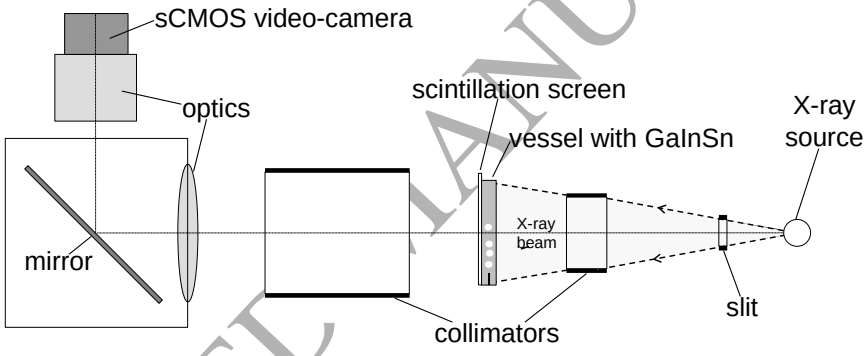


Figure 1. Experimental setup.

**Results and discussion**

A variety of experiments were performed for different gas flow rates up to 1200 cm$^3$/min. Single bubbles detach from the injection nozzle forming a bubble chain for Ar gas flow rates below 800 cm$^3$/min, while the bubbles are ejected as clusters at higher gas flow rates. The total experimental time and bubble release frequency from the injection nozzle can be found in Table 1. The bubble size increases with increasing Ar volume flow rate; while the bubble ejection frequency remains almost constant within the measurement uncertainty. Due to flow instabilities and the resulting formation of vortices the bubble chain becomes curved in form of an S-shape which is typical for a narrow configuration of the container and for the chosen aspect ratio of the fluid. In contrast to coalescence (Keplinger et al., 2018), bubble breakup appears first at a gas flow rate of 400 cm$^3$/min with ~0.017 breakup events per second and grows continuously to ~0.55 breakup events per second for gas flow rates up to 700 cm$^3$/min (see Table 1). The onset of bubble breakup can be related to increasing surface deformations experienced by the bubbles with increasing bubble size. Bubble breakup in this study leads predominantly to the formation of two daughter bubbles. For 800 cm$^3$/min the number of bubble breakup events slightly decreases to about 0.5 breakup events per second. However, it must be mentioned here that due to bubble clustering the number of

breakup events cannot be accurately counted at higher gas flow rates. Moreover, it should be noticed that the spatial resolution of the experimental method can only detect bubbles with diameters greater than 1 mm. This limitation could in turn lead to an underestimation of the bubble breakup frequency. However, in this regard, the large surface tension of the liquid metals is advantageous in terms of avoiding a breakup in many tiny daughter bubbles.

| Gas flow rate ($cm^3$/min) | 400 | 500 | 600 | 700 | 800 |
|---|---|---|---|---|---|
| Total experimental time (s) | 114,68 | 115,28 | 95,68 | 109,93 | 110,64 |
| Bubble ejection frequency (bubbles/s) | 34±4 | 31.5±3.5 | 32.5±3.5 | 35±3 | 34.5±5.5 |
| Bubble diameter calculated from bubble ejection frequency and gas flow rate (mm) | 6.9-7.5 | 7.7-8.3 | 8.1-8.7 | 8.4-8.9 | 8.8-9.8 |
| Total number of bubble breakup events per second | 0.017 | 0.25 | 0.44 | 0.55 | 0.5 |
| Number of bubble breakup events per second initiated by bubble-bubble interaction | 0.017 | 0.25 | 0.31 | 0.47 | 0.45 |
| Number of bubble breakup events per second initiated by stretching | - | - | 0.13 | 0.08 | 0.05 |

Table 1. Total experimental time, bubble ejection frequency, bubble diameter and number of bubble breakup events per second for the middle area of 55×120$mm^2$ above the bottom of the container.

Figure 2 shows the time-averaged brightness obtained from about 10000 consecutive single X-ray images for 400 $cm^3$/min (a), 500 $cm^3$/min (b), 600 $cm^3$/min (c), 700 $cm^3$/min (d) and 800 $cm^3$/min (e). It becomes obvious that due to the bevel shape of the orifice the bubble chain has a preferential path and the bubble chain is deflected to the right. A much broader bubble distribution can be observed for 700 $cm^3$/min and 800 $cm^3$/min (see Figures 2d and 2e) which is a result of bubble chain oscillations in the observation plane (see also Liu et al., 2018). The rising gas bubbles induce a turbulent flow inside the container. The highest turbulence level is generated along the bubble path, near the free surface and near the side walls of the vessel (Krull et al., 2017; Liu et al., 2018). Since the turbulent flow is not homogeneous it is important to discuss the positions at which the breakup events occur. The crosses in Figures 2 a-e indicate the bubble breakup positions. It can be seen that the bubble breakup events are most likely to appear in the upper part of the container while no breakage is observed in the near-nozzle region. In this region the bubble distance is dominated by the bubble injection frequency and the bubbles move as isolated objects with rarely appearing bubble collisions (B. Krull et al., 2017). In comparison to the upper part of the container the near-nozzle region can be characterized by a rather narrow distribution of fluid velocities and a low turbulence level (see for instance simulations by Krull et al. (2017) and Liu et al. ( 2018)). Additionally, the broader bubble distributions for high gas flow rates lead to a larger scatter of the bubble breakup positions (see Figure 2 d and e).

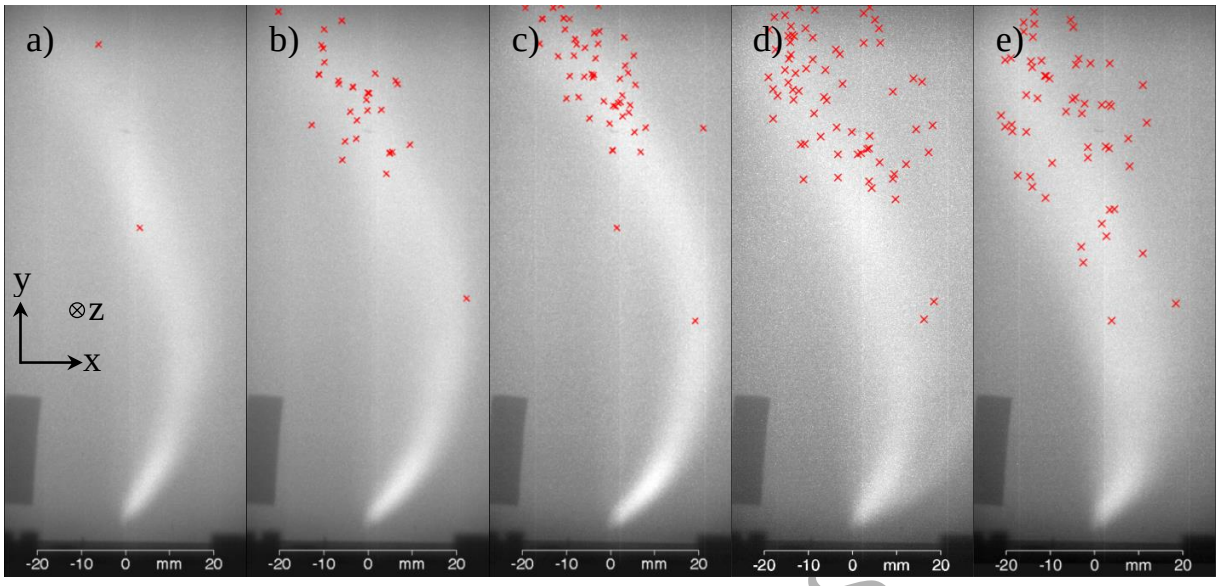


Figure 2. Time-averaged brightness obtained from about 10000 consecutive single X-ray images (the related measurement times can be found in Table 1) with marked bubble breakup positions for 400 $cm^3$/min (a), 500 $cm^3$/min (b), 600 $cm^3$/min (c), 700 $cm^3$/min (d) and 800 $cm^3$/min (e). The observation window is 55×130$mm^2$.

Most bubble breakup events observed in our experimental geometry occur as a result of the interaction of the bubble with its pursuing bubble (see Table 1). Such interactions are typical for the bubble pairing regime which is characterized by the fact that the initially equidistant bubble chain starts to disintegrate when leaving the near-nozzle region and two consecutive bubbles form a pair (Badam et al., 2008; Fan and Tsuchiya, 1990; Kyriakides et al., 1997). Bubble interaction leading to breakage is either governed by bubble collision or by flow modifications (e.g. by bubble-eddy collisions or turbulent shear) induced by the small distance and the relative velocity of the bubbles. In addition, the influence of the global flow inside the vessel cannot be completely omitted. A typical example for such a breakage is shown in Figure 3a. During the first frames the trailing bubble is accelerated in the wake of the leading one (see also Video1.avi of the supplementary material). As a result the trailing bubble quickly approaches the leading one and the bubbles collide (frame 1, t = 4.41 s). The leading bubble flattens and the bubbles start to rise as a cluster being separated by a thin liquid film for several frames (frames 1-4, t = 4.41-4.44 s). During the collision the leading bubble expands in the plane of view and finally breaks into two smaller bubbles (frame 5, t = 4.45 s). After the breakage the bubble fragment rise independently (frames 5-7).

Other breakups are governed by bubble stretching only (see Table 1). In this case the breaking bubble can be considered as an isolated one since the distance to the neighboring bubbles remains large enough to exclude bubble collisions and interactions. Such a condition inside a bubble chain is only guaranteed when the bubbles do not strongly interact with the wakes of preceding bubbles. An example of such a breakage is demonstrated in Figure 3b (see also Video2.avi of the supplementary material). The bubble size in this case is 10±0.2 mm. In addition, Figure 3c shows the corresponding evolution of the bubble surface during the rise. The background of Figure 3c represents the time-averaged brightness of X-ray images over a period of 4 s prior to breakup. It becomes obvious that in this case the bubble undergoes strong deformations which are caused by the highly turbulent shear flow generated by the rising bubbles in the path region. In this example, the bubble is distinctly stretched due to the considerable local velocity gradient: the right part of the bubble reaches into the low velocity region outside the main bubble path

while the left part of the bubble is near the center of the main bubble path, where the highest velocities occur (Figure 3b frames 1-3 and Figure 3c). As a consequence, shear viscous forces tear the bubble apart causing its breakage (Figure 3b frames 4). In this case, the shear stress acting on the bubble can be calculated as

$$\tau = \mu \frac{\Delta v}{\Delta l}, \quad (6)$$

where $\mu$ = 2.09 mPa·s is the dynamic viscosity of GaInSn at room temperature (see Plevachuk et al., (2014) for details), $\Delta v$ is the velocity difference and $\Delta l$ is the distance between the left and the right side of the bubble. When $\tau$=0 both bubble sides move at the same rising velocity; if $\tau$ becomes positive the left side of the bubble moves faster than the right one and vice versa. A simple estimation of the maximum shear stress that the bubble experiences in this case reveals a value of ~0.1 mPa 0.07 s before the breakup occurs (see Figure 4a where time step "0" indicates the moment of breakage) and corresponds to the transition between the two bubble snapshots A and B indicated in Figure 3c. The bubble snapshots A and B are characterized by an almost spherical shape with a negligible bubble deformation ($A^*$) of ~1.01 and 1.035, respectively (Figure 4b). Also, 0.03 s before this transition the right part of the bubble starts to decelerate from 0.7 m/s down to 0.33 m/s, meanwhile the left part of the bubble starts to accelerate from 0.42 m/s up to 0.7 m/s (Figure 4c). This in turn indicates the moment when the right part of the bubble becomes affected by the slower moving liquid outside the bubble path. After reaching the maximum velocity difference of 0.6 m/s at the transition between the time steps A and B, the movement of both sides of the bubble slows down considerably. At the same time, although the difference of 0.2 m/s in the velocities is maintained, the degree of bubble deformation increases greatly ultimately leading to breakup (Figure 3b, frame 4). Right before the breakage occurs, the shear stress value is $\tau$ ~ 0.02 mPa (Figure 4a).

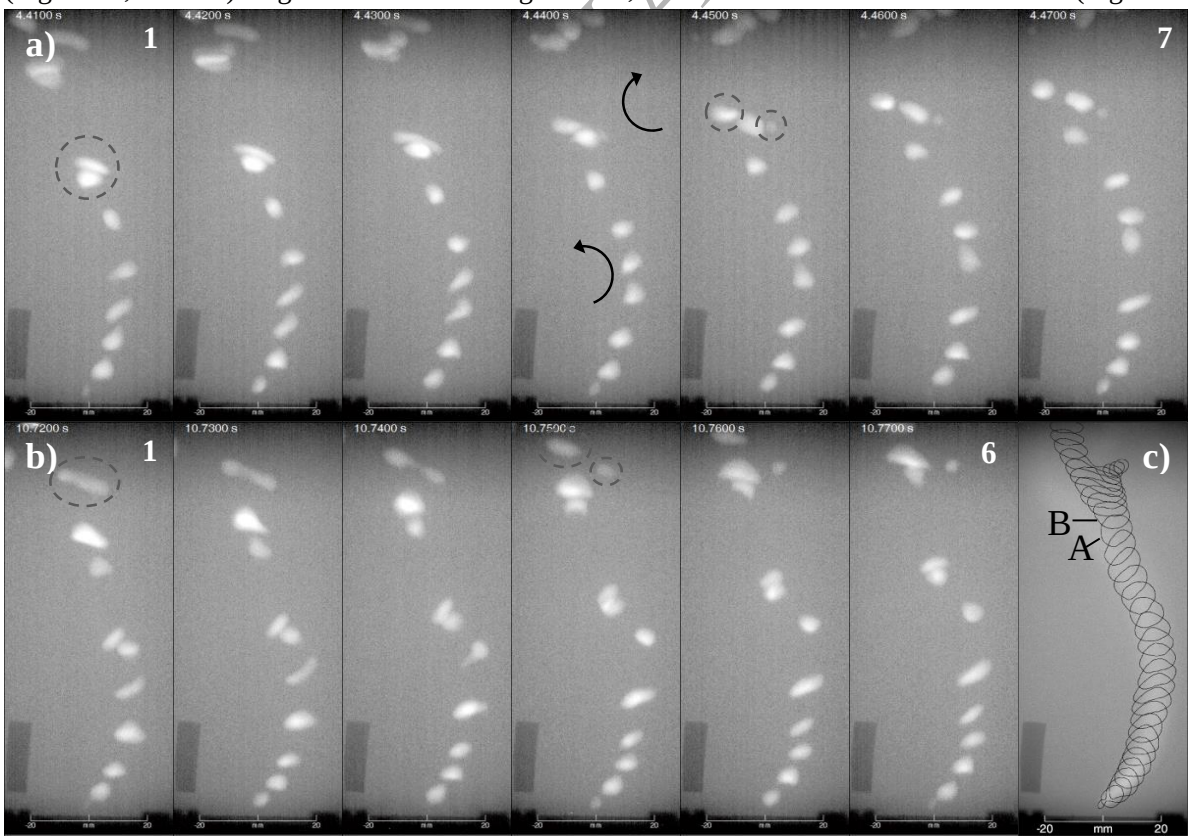

Figure 3. Sequence of single frames illustrating: a) bubble breakup initiated by collision of two single bubbles, b) single bubble breakup caused by bubble stretching. c) Evolution of the bubble surface during rise for the case demonstrated in Figure 3b. Time step between two frames is 0.01 s. Ar gas flow rate in both cases is 600 $cm^3$/min.

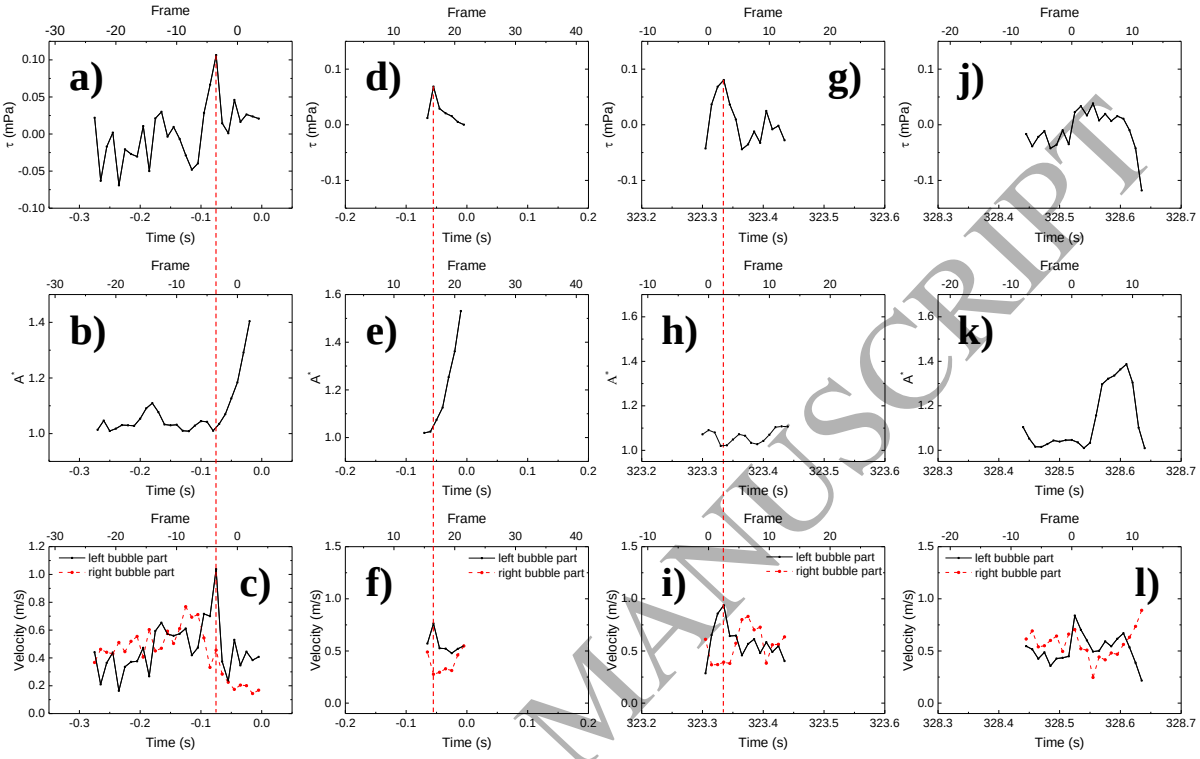


Figure 4. Shear stress (a), bubble deformation (b) and bubble velocities (c) for case shown in Figure 3b. Shear stress (d), bubble deformation (e) and bubble velocities (f) for case shown in Figure 5. Shear stress (g), bubble deformation (h) and bubble velocities (i) for case shown in Figure 7. Shear stress (j), bubble deformation (k) and bubble velocities (l) for case shown in Figure 8. Vertical dashed lines indicate the position of the maximum shear stress. Time step '0' in figures a-f indicates the moment of breakage.

Since X-ray radiography provides only two-dimensional information it is rather hard to accurately determine the bubble collision geometry. In addition, the flow structure in the liquid cannot be determined either by the X-ray radiography. Therefore, it is difficult to judge whether the breakage is mainly governed by bubble collision or by the collision with local turbulence. In view of these uncertainties, it was decided to restrict the further quantitative analysis to the case of isolated bubbles whose breakage is a result of stretching. The distance to the neighboring bubbles at the moment of breakage is at least several mm so that the influence of the neighboring bubbles on the breakup can be neglected.

Bubble breakup induced by bubble stretching is observed for gas flow rates above 600 $cm^3$/min (see Table 1). The probability of bubble breakup by stretching decreases at lower gas flow rates because the tendency for bubble deformation also decreases with decreasing bubble size. In addition, the high surface tension of the liquid metal counteracts any deformation of the bubble interface. The rising bubbles generate turbulence inside the container. The turbulence intensity depends strongly both on the bubble ejection frequency and the bubble size: the larger the bubble the stronger the local flow fluctuations (see for instance Liu et al. (2018)). Additionally, the distribution of large bubbles is significantly more

dispersed compared to smaller bubbles. This also extends the zone of bubble-induced turbulence. In turn, one could deduce that larger gas bubbles statistically more often fall into areas of high velocity gradients.

In addition to the two mechanisms discussed so far, events of the bubble breakup are also observed in which coalescence plays an essential role as an intermediate stage. Coalescence occurs frequently in the bubble pairing regime at high gas flow rates (Keplinger et al., 2018). Such an example is shown in Figure 5 (the entire bubble rising process can be viewed in the Video3.avi of the supplementary material). Frame 28 in Figure 5 shows the corresponding evolution of the bubble surface during the rise. The background represents the time-averaged brightness of X-ray images over a period of 4 s prior to breakup. At the beginning of the sequence two consecutively ejected bubbles of 8.2±0.2 mm size come closer to each other and collide (frames 1-14) resulting in coalescence which is associated with an increase in the bubble size (frame 15, also indicated as bubble snapshot C in frame 28). Frame 28 clearly demonstrates that, as in the previous case presented in Figure 3, the bubble gets under the influence of strong velocity gradients resulting in bubble elongation, surface indentation and necking (frames 19-21) and finally breaks into two daughter bubbles (frame 22). The merged bubble deforms from an almost spherical shape ($A^* = 1.02$, frame 15) to an elongated one ($A^* = 1.53$, frame 21). The highest value of the shear stress (~0.07 mPa) was detected between the frames 16 and 17 (see Figure 4d where time step "0" indicates the moment of breakage) as a result of a increasing velocity of the left bubble part with a simultaneous slowed down movement of the right bubble part leading to a velocity difference of almost 0.5 m/s (Figure 4f). Here too, achieving such a maximum is followed by a distinct reduction of both the mean bubble velocity and the velocity difference between both bubble sides. Thus, the shear stress almost disappears just before the bubble breaks apart. In the present case, the bubble breaks into two fragments of unequal size which move independently after breakup: the bigger bubble fragment follows the main bubble rising trajectory, while the smaller fragment ascends almost straightly upwards (see frames 24-28).

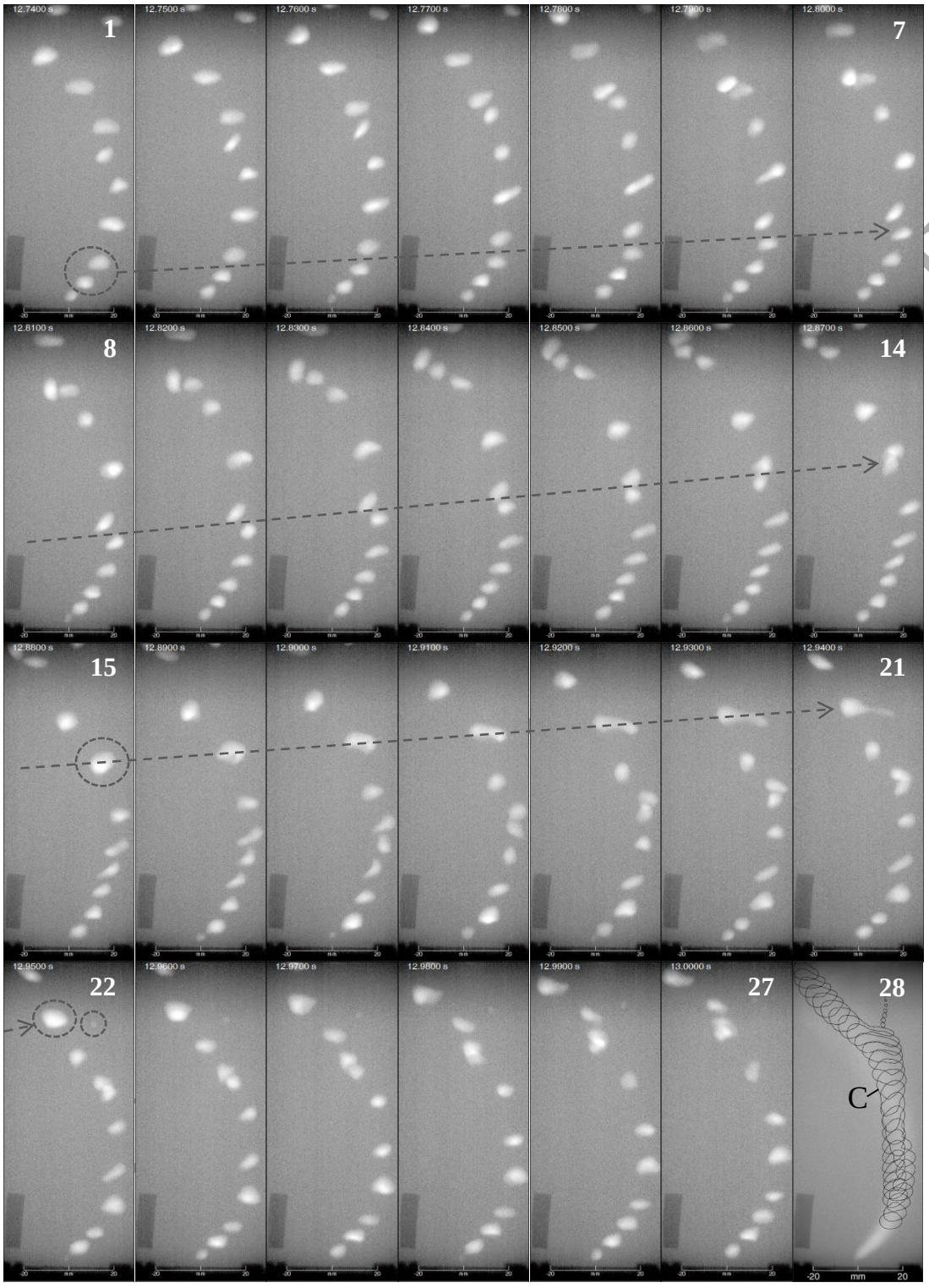


Figure 5. Sequence of single frames illustrating bubble coalescence with subsequent breakup initiated by stretching at a gas flow rate of 600 $cm^3$/min. Time step between two frames is 0.01 s. Frame 28: evolution of the bubble surface.

Figure 6 presents the results for trajectories, deformation, bubble size and velocity for all bubble breakups caused by stretching at gas flow rates of 600-800 $cm^3$/min. This figure also includes the events where coalescence occurred. The data of the original bubbles are plotted in black whereas the light green and light blue colors indicate the daughter bubbles. In the case of coalescence, the data of the original trailing bubble and the coalesced bubble are marked red and dark blue, respectively. Time step "0" corresponds to the moment when the bubble breaks into two daughters. Figure 6a shows that the bubble breakup caused by stretching only appears at the upper part of the container (at a height above 93.4 mm). Figure 6b demonstrates that the bubbles are veritably deformed (up to 1.16) as soon as they have left the nozzle which is a result of rather high Reynolds ($Re = \frac{\rho u d}{\mu} \approx 7600$ for a 10 mm bubble rising in GaInSn at a terminal velocity of 0.25 m/s) and small Morton ($Mo = \frac{g\mu^4}{\rho\sigma^3} \approx 2\times10^{-13}$, where g is the acceleration of gravity) numbers. The deformation further increases during the rise of the bubbles till the breakup occurs. The onset of breakup seems to require a minimum deformation value of about ~1.38 (see Figure 6b). The evolution of the bubble sizes is presented in Figure 6c. It becomes obvious that bubble breakup occurs in the majority of cases only at bubble diameters $d_B \geq 9.8\pm0.2$ mm. Nevertheless, one bubble breakup event was observed for a smaller bubble with a size of $d_B = 7.7\pm0.2$ mm. Figure 6d reveals a maximum of the bubble velocity before breakup corresponding to the particular behavior of the shear stress as shown in Figure 4 a and d. The breakup events that we observed resulted in the formation of a maximum of two daughter bubbles, while in most cases their size differed significantly.

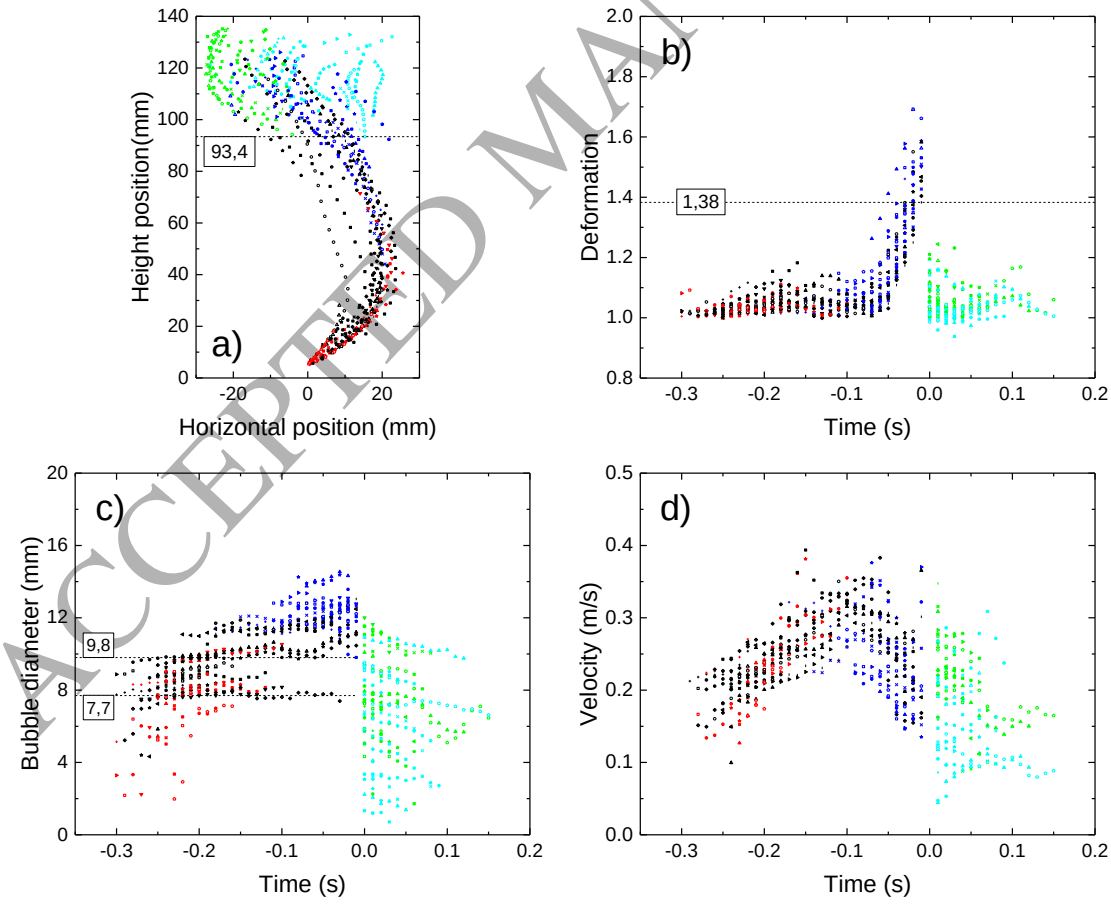

Figure 6. Bubble trajectories (a), bubble deformations (b), bubble diameters (c) and bubble velocities (d) before and after breakup. The numbers indicate the minimum values at which the bubble breakup was observed. The data of the original bubbles are plotted in black whereas the light green and light blue colors indicate the daughter bubbles. In the case of coalescence, the data of the original trailing bubble and the coalesced bubble are marked red and dark blue, respectively.

When moving upwards not all bubbles undergo a strong deformation which leads to the breakup. A simple example of such a case is demonstrated in Figure 7. The entire bubble rising process can be viewed in the Video4.avi of the supplementary material. Frame 14 in Figure 7 shows the evolution of the bubble surface during the rise with D indicating the moment of bubble coalescence. During the first frames (here not shown) two smaller bubbles merge into one forming a bubble of 13.1±0.2 mm size. Despite the point that the right part of the bubble ends up outside the main bubble path the bubble motion can be characterized by rather low deformation values ($A^*$) lying in the range of 1.02-1.11 (see Figure 4h). The maximum shear stress felt by the bubble equals to ~0.08 mPa (see Figure 4g) and is reached during transition between frames 2 and 3 in Figure 7. This situation is also characterized by a larger velocity of the left side of the bubble which is similar to the previous two cases (see Figure 4i). Due to insufficient deformation (Figure 4h) the bubble leaves the FOV without breaking. Nevertheless, the breakage might still appear at a later rising stage close to the free surface. On the other hand, the point that the bubble is not breaking in the FOV might be explained either by rather week turbulence insufficient to cause deformation required for breakage or by the interaction with the side walls which is relevant for coalesced bubbles of such size.

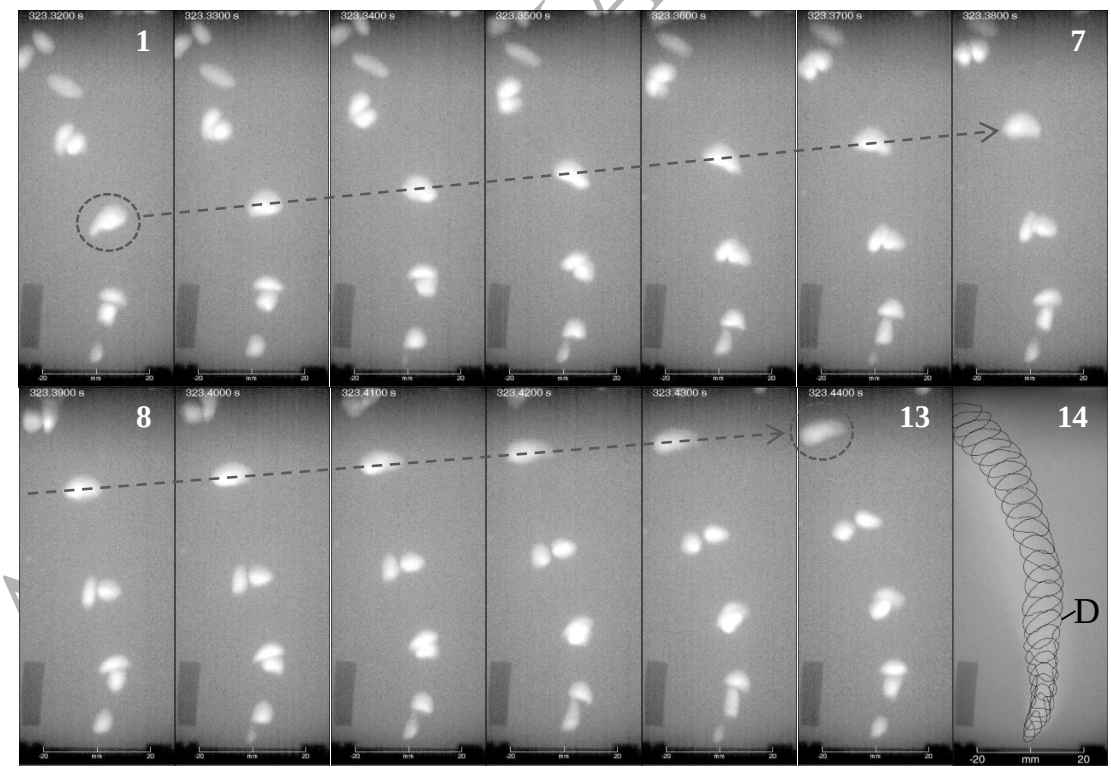


Figure 7. Bubble motion without breakup for 800 $cm^3$/min. Time step between two frames is 0.01 s. Frame 14: evolution of the bubble surface during rise.

Another example which illustrates a case when a single bubble undergoes strong deformation in the upper part of the vessel but does not break is shown in Figure 8. The entire bubble rising process can be viewed in the Video5.avi of the supplementary material. Frame 14 in Figure 8 shows the evolution of the bubble surface during the rise. The bubble size in this case is 10.8±0.2 mm and the maximum deformation the bubble undergoes in frame 9 and is ~1.39 (see also Figure 4k). In comparison to the previous cases the main bubble deformations take place within the main bubble path (i.e. no bubble parts move outside the main bubble path). The shear stress in this case only shows a deep decline (Figure 4j) at the moment when the right part of the bubble starts to move faster than the left one and the bubble contracts (frames 10-13) taking a more spherical-like shape with $A^* = 1.01$ (frame 12). In general, such a bubble contraction is a direct result of the large surface tension for GaInSn which tries to keep the bubble as a unit. It occurs if the turbulence impact on the bubble is weak. Nevertheless, influence of the side walls cannot be completely neglected.

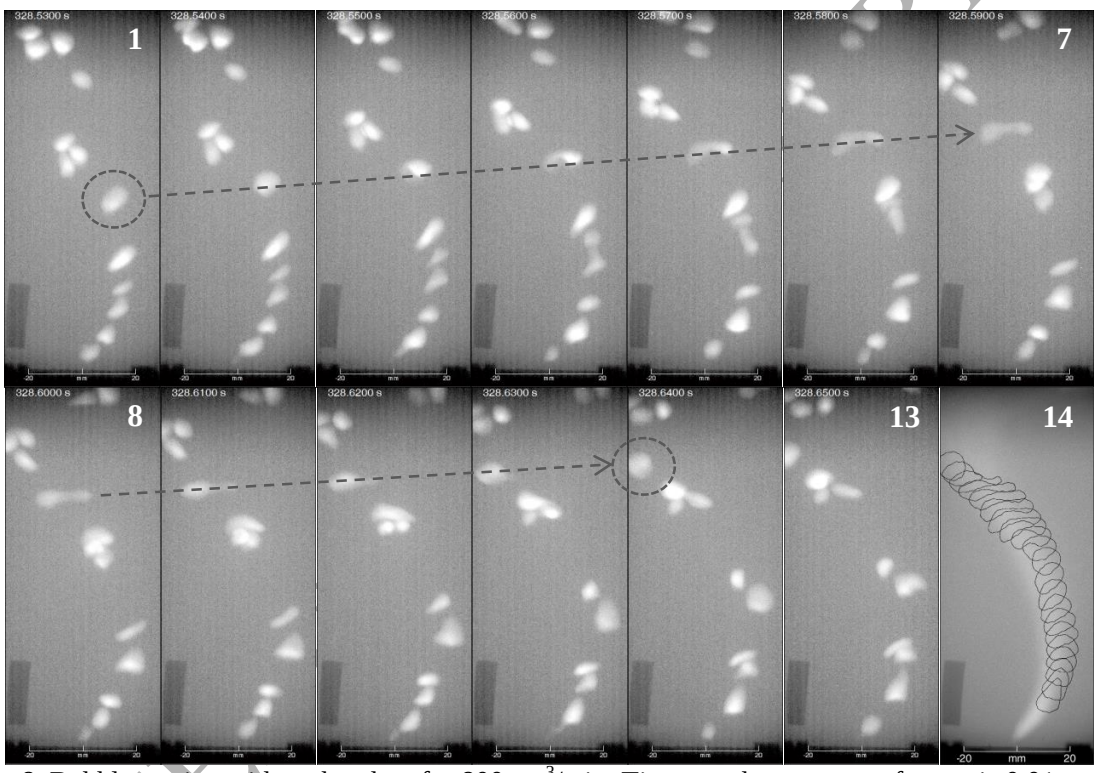


Figure 8. Bubble motion without breakup for 800 $cm^3$/min. Time step between two frames is 0.01 s. Frame 14: evolution of the bubble surface during rise.

**Conclusions**

For the first time, an experimental investigation of bubble breakup in opaque liquid metals has been performed by means of high-speed video imaging using X-ray radiography. The analysis of the X-ray images allows for determining bubble trajectories, size, shape and velocity. It has to be noticed that the analysis is limited to two-dimensional images, although the processes are determined by three-dimensional effects. The parameter range considered here differs significantly from bubbly flows in water and highly viscous fluids which have been extensively studied in previous papers.

Qualitative evaluation reveals that the majority of the breakup events in a bubble chain are caused by interaction with trailing bubbles. In this case the breakage is either provoked by bubble collision or by the

local flow modifications due to the close motion of the trailing bubble. The onset of this breakup regime is observed at gas flow rates of 400 $cm^3$/min when bubble pairing occurs. The number of breakup events grows continuously with increasing gas flow rate. A second breakup regime appearing at gas flow rates ≥ 600 $cm^3$/min is governed by bubble stretching only and decreases with increasing gas flow rate. The decrease is related to enhanced bubble pairing for high gas flow rates. Quantitative analysis of bubble breakup has been restricted to the stretching mechanism because of the limitations of the X-ray technique and the fact that such a restriction allows reducing the number of processes that might be responsible for breakage.

The bubble breakup induced by stretching can be attributed to the influence of the liquid turbulence on the bubble. The gas-liquid interface is exposed to a significant shear stress due to strong local velocity gradients and the highly fluctuating flow. When the bubble moves under the influence of strong velocity gradients, parts of the bubble experience different velocities of the ambient liquid. The corresponding modification of the pressure field leads to a deformation of the bubble which could result in breakup. It is interesting to note that a significant peak of the velocity gradient or the related shear force along the bubble is observed before the bubble motion is decelerated and breakup occurs.

Our experiments show the occurrence of breakup for bubbles with sizes of $d_B \geq 9.8 \pm 0.2$ mm at Reynolds numbers of $Re \geq 7500$. Moreover, it became obvious that a minimum deformation value of 1.38 is required for breakup. In comparison, studies in air-water systems observed bubble breakup for significantly smaller gas bubbles at $d_B \geq 3$ mm and Reynolds numbers of Re ≥ 4000 (Brandner et al., 2015; Solsvik and Jakobsen, 2015b; Vejražka et al., 2017). Risso and Fabre (1998) reported breakup under microgravity conditions for bubbles with $d_B \geq 12.4$ mm. They also obtained a universal *We* number of about 5 and have concluded that the Weber number is responsible for the bubble deformation but the turbulence plays a deciding role for breakage since it supplies the amount of energy lacking to obtain the breakup of the pre-deformed bubble. The Weber numbers in our experiments (considering an average terminal velocity of 0.25 m/s) yield values of $We \geq 6.6$.

In contrast to water where breakups result usually in the formation of multiple daughters (Brandner et al., 2015; Risso and Fabre, 1998; Solsvik and Jakobsen, 2015b; Vejražka et al., 2017) bubble breakups in GaInSn lead to the formation of only two daughters. After breakage the formation of two unequally sized fragments is dominant which is similar to the observations by Hesketh et al. ( 1991) and Andersson and Andersson (2006) for air bubbles in water.

Comparison to a case when the bubble undergoes significant deformation without breakup does not reveal significant differences in the parameters which allow for identifying a quantitative criterion for breakup. The highest bubble deformation for the case without breakage was 1.39, whereas a minimum values of 1.38 (the threshold value for $A^*$) were found for the breakup cases. Therefore, it can be concluded that the bubble deformation is seemingly not the only effective parameter for describing breakup. The only significant difference was that in case of a breakage the shear stress showed a peak right before the bubble started to deform continuously. Nevertheless, even a peak in shear stress is not a guaranty for breakup since it is not always coupled with a remarkable bubble deformation. Our experiments were conducted in the turbulent regime and due to insignificant differences in parameters for breaking and not breaking bubbles we assume that the processes of breakup are mainly governed by the structure of the turbulent flow in the vicinity of the bubbles. In other words, it can also be said that the mentioned minimum criteria with respect to the bubble size, shear force and bubble deformation can be interpreted as thresholds being necessary but not sufficient to achieve bubble breakup. Also due to the narrow configuration of the container the influence of the walls on the breakage process cannot be

completely neglected. In case of bubbles with $d_B \geq 12$ mm the walls might play a major role in compensating the turbulence impact which could confine the extent of the bubble deformation.

**Acknowledgments**

The authors are grateful to the German Helmholtz Association for the financial support in form of the Helmholtz-Alliance "LIMTECH".

**Literature**

Andersson, R., Andersson, B., 2006. On the breakup of fluid particles in turbulent flows. AIChE J. 52, 2020–2030. https://doi.org/10.1002/aic.10831

Baake, E., Fehling, T., Musaeva, D., Steinberg, T., 2017. Neutron radiography for visualization of liquid metal processes: bubbly flow for $CO_2$ free production of Hydrogen and solidification processes in EM field. IOP Conf. Ser. Mater. Sci. Eng. 228, 012026. https://doi.org/10.1088/1757-899X/228/1/012026

Badam, V.K., Buwa, V., Durst, F., 2008. Experimental investigations of regimes of bubble formation on submerged orifices under constant flow condition. Can. J. Chem. Eng. 85, 257–267. https://doi.org/10.1002/cjce.5450850301

Brandner, P.A., Henderson, A.D., De Graaf, K.L., Pearce, B.W., 2015. Bubble breakup in a turbulent shear layer. J. Phys. Conf. Ser 656, 012015. https://doi.org/doi:10.1088/1742-6596/656/1/012015

Chatzi, E., Lee, J.M., 1987. Analysis of interactions for liquid-liquid dispersions in agitated vessels. Ind. Eng. Chem. Res. 26, 2263–2267. https://doi.org/10.1021/ie00071a016

Chatzi, E.G., Gavrielides, A.D., Kiparissides, C., 1989. Generalized model for prediction of the steady-state drop size distributions in batch stirred vessels. Ind. Eng. Chem. Res. 28, 1704–1711. https://doi.org/10.1021/ie00095a022

Chen, P., Duduković, M.P., Sanyal, J., 2005. Three-dimensional simulation of bubble column flows with bubble coalescence and breakup. AIChE J. 51, 696–712. https://doi.org/10.1002/aic.10381

Clift, R., Grace, J.R., Weber, M.E., 1978. Bubbles, Drops, and Particles. Acad. Press.

Coulaloglou, C.A., Tavlarides, L.L., 1977. Description of interaction processes in agitated liquid-liquid dispersions. Chem. Eng. Sci. 32, 1289–1297. https://doi.org/10.1016/0009-2509(77)85023-9

Davis, K.G., Irons, G.A., Guthrie, R.I.L., 1978. X-Ray Cinematographic Observations of Gas Injection into Liquid Metals. Metall. Trans. B 9, 721–722. https://doi.org/10.1007/BF03257224

Eckert, S., Gerbeth, G., Lielausis, O., 2000a. The behaviour of gas bubbles in a turbulent liquid metal magnetohydrodynamic flow: Part I: Dispersion in quasi-two-dimensional magnetohydrodynamic turbulence. Int. J. Multiph. Flow 26, 45–66. https://doi.org/10.1016/S0301-9322(99)00006-3

Eckert, S., Gerbeth, G., Lielausis, O., 2000b. The behaviour of gas bubbles in a turbulent liquid metal magnetohydrodynamic flow: Part II: Magnetic field influence on the slip ratio. Int. J. Multiph. Flow 26, 67–82. https://doi.org/10.1016/S0301-9322(99)00007-5

Fan, L.-S., Tsuchiya, K., 1990. Bubble wake dynamics in liquids and liquid-solid suspensions. Butterworth-Heinemann.

Fröhlich, J., Schwarz, S., Heitkam, S., Santarelli, C., Zhang, C., Vogt, T., Boden, S., Andruszkiewicz, A., Eckert, K., Odenbach, S., Eckert, S., 2013. Influence of magnetic fields on the behavior of bubbles in liquid metals. Eur. Phys. J. Spec. Top. 220, 167–183. https://doi.org/10.1140/epjst/e2013-01805-4

Fu, X.., Ishii, M., 2003. Two-group interfacial area transport in vertical air–water flow: I. Mechanistic model. Nucl. Eng. Des. 219, 143–168. https://doi.org/10.1016/S0029-5493(02)00285-6

Gundrum, T., Büttner, P., Dekdouk, B., Peyton, A., Wondrak, T., Galindo, V., Eckert, S., 2016. Contactless Inductive Bubble Detection in a Liquid Metal Flow. Sensors 16, 63. https://doi.org/10.3390/s16010063

Heindel, T.J., 2011. A Review of X-Ray Flow Visualization With Applications to Multiphase Flows. J.

Fluids Eng. 133, 074001. https://doi.org/10.1115/1.4004367
Hesketh, R.P., Etchells, A.W., Russell, T.W.F., 1991. Experimental observations of bubble breakage in turbulent flow. Ind. Eng. Chem. Res. 30, 835–841. https://doi.org/10.1021/ie00053a005
Iguchi, M., Chihara, T., Takanashi, N., Ogawa, Y., Tokumitsu, N., Morita, Z., 1995. X-ray Fluoroscopic Observation of Bubble Characteristics in a Molten Iron Bath. ISIJ Int. 35, 1354–1361. https://doi.org/10.2355/isijinternational.35.1354
Iguchi, M., Nakatani, T., Kawabata, H., 1997. Development of a multineedle electroresistivity probe for measuring bubble characteristics in molten metal baths. Metall. Mater. Trans. B 28, 409–416. https://doi.org/10.1007/s11663-997-0106-3
Kastengren, A., Powell, C.F., 2014. Synchrotron X-ray techniques for fluid dynamics. Exp. Fluids 55, 1686. https://doi.org/10.1007/s00348-014-1686-8
Keplinger, O., Shevchenko, N., Eckert, S., 2018. Visualization of bubble coalescence in bubble chains rising in a liquid metal. Int. J. Multiph. Flow 105, 159–169. https://doi.org/10.1016/J.IJMULTIPHASEFLOW.2018.04.001
Keplinger, O., Shevchenko, N., Eckert, S., 2017. Validation of X-ray radiography for characterization of gas bubbles in liquid metals. IOP Conf. Ser. Mater. Sci. Eng. 228, 012009. https://doi.org/10.1088/1757-899X/228/1/012009
Kitscha, J., Kocamustafaogullari, G., 1989. Breakup criteria for fluid particles. Int. J. Multiph. Flow 15, 573–588. https://doi.org/10.1016/0301-9322(89)90054-2
Kocamustafaogullari, G., Ishii, M., 1995. Foundation of the interfacial area transport equation and its closure relations. Int. J. Heat Mass Transf. 38, 481–493. https://doi.org/10.1016/0017-9310(94)00183-V
Krishna, R., Urseanu, M.I., van Baten, J.M., Ellenberger, J., 1999. Wall effects on the rise of single gas bubbles in liquids. Int. Commun. Heat Mass Transf. 26, 781–790. https://doi.org/10.1016/S0735-1933(99)00066-4
Krull, B., Strumpf, E., Keplinger, O., Shevchenko, N., Fröhlich, J., Eckert, S., Gerbeth, G., 2017. Combined experimental and numerical analysis of a bubbly liquid metal flow. IOP Conf. Ser. Mater. Sci. Eng. 228, 012006. https://doi.org/10.1088/1757-899X/228/1/012006
Kyriakides, N.K., Kastrinakis, E.G., Nychas, S.G., Goulas, A., 1997. Bubbling from nozzles submerged in water: Transitions between bubbling regimes. Can. J. Chem. Eng. 75, 684–691. https://doi.org/10.1002/cjce.5450750405
Lee, C.-H., Erickson, L.E., Glasgow, L.A., 1987a. Bubble breakup and coalescence in turbulent gas-liquid dispersions. Chem. Eng. Comm 59, 65–84.
Lee, C.-H., Erickson, L.E., Glasgow, L.A., 1987b. Dynamics of bubble size distribution in turbulent gas-liquid dispersions. Chem. Eng. Comm 61, 181–195.
Lehr, F., Millies, M., Mewes, D., 2002. Bubble-Size distributions and flow fields in bubble columns. AIChE J. 48, 2426–2443. https://doi.org/10.1002/aic.690481103
Liao, Y., Lucas, D., 2009a. A literature review of theoretical models for drop and bubble breakup in turbulent dispersions. Chem. Eng. Sci. 64, 3389–3406. https://doi.org/10.1016/j.ces.2009.04.026
Liao, Y., Lucas, D., 2009b. A literature review of theoretical models for drop and bubble breakup in turbulent dispersions. Chem. Eng. Sci. 64, 3389–3406. https://doi.org/10.1016/j.ces.2009.04.026
Liao, Y., Rzehak, R., Lucas, D., Krepper, E., 2015. Baseline closure model for dispersed bubbly flow: Bubble coalescence and breakup. Chem. Eng. Sci. 122, 336–349. https://doi.org/10.1016/j.ces.2014.09.042
Liu, L., Keplinger, O., Ma, T., Ziegenhein, T., Shevchenko, N., Eckert, S., Yan, H., Lucas, D., 2018. Euler-Euler simulation and X-ray measurement of bubble chain in a shallow container filled with liquid metals. Chem. Eng. Sci. 192, 288–305. https://doi.org/10.1016/J.CES.2018.07.034
Luo, H., Svendsen, H.F., 1996. Theoretical model for drop and bubble breakup in turbulent dispersions. AIChE J. 42, 1225–1233. https://doi.org/10.1002/aic.690420505
Lyu, Z., Karcher, C., 2016. Experimental study on bubble rising in liquid GaInSn using Local Lorentz Force Velocimetry (LLFV). Proc. 10th PAMIR Int. Conf. Fundam. Appl. MHD (Cagliary, Italy) 243–246.

Manera, A., Ozar, B., Paranjape, S., Ishii, M., Prasser, H.-M., 2009. Comparison between wire-mesh sensors and conductive needle-probes for measurements of two-phase flow parameters. Nucl. Eng. Des. 239, 1718–1724. https://doi.org/10.1016/j.nucengdes.2008.06.015

Martín, M., Montes, F.J., Galán, M.A., 2008. Influence of Impeller Type on the Bubble Breakup Process in Stirred Tanks. Ind. Eng. Chem. Res. 47, 6251–6263. https://doi.org/10.1021/ie800063v

Martínez-Bazán, C., Montañés, J.L., Lasheras, J.C., 1999a. On the breakup of an air bubble injected into a fully developed turbulent flow. Part 1. Breakup frequency. J. Fluid Mech. 401, S0022112099006680. https://doi.org/10.1017/S0022112099006680

Martínez-Bazán, C., Montañés, J.L., Lasheras, J.C., 1999b. On the breakup of an air bubble injected into a fully developed turbulent flow. Part 2. Size PDF of the resulting daughter bubbles. J. Fluid Mech. 401, S0022112099006692. https://doi.org/10.1017/S0022112099006692

Mishima, K., Hibiki, T., Saito, Y., Nishihara, H., Tobita, Y., Konishi, K., Matsubayashi, M., 1999. Visualization and measurement of gas-liquid metal two-phase flow with large density difference using thermal neutrons as microscopic probes. Nucl. Instruments Methods Phys. Res. Sect. A Accel. Spectrometers, Detect. Assoc. Equip. 424, 229–234. https://doi.org/10.1016/S0168-9002(98)01300-X

Mudde, R.F., 2010. Advanced measurement techniques for GLS reactors. Can. J. Chem. Eng. 88, n/a-n/a. https://doi.org/10.1002/cjce.20315

Mudde, R.F., Alles, J., van der Hagen, T.H.J.J., 2008. Feasibility study of a time-resolving x-ray tomographic system. Meas. Sci. Technol. 19, 085501. https://doi.org/10.1088/0957-0233/19/8/085501

Oryall, G.N., Brimacombe, J.K., 1976. The physical behavior of a gas jet injected horizontally into liquid metal. Metall. Trans. B 7, 391–403. https://doi.org/10.1007/BF02652710

Plevachuk, Y., Sklyarchuk, V., Eckert, S., Gerbeth, G., Novakovic, R., 2014. Thermophysical Properties of the Liquid Ga–In–Sn Eutectic Alloy. J. Chem. Eng. Data 59, 757–763. https://doi.org/10.1021/je400882q

Prince, M.J., Blanch, H.W., 1990. Bubble coalescence and break-up in air-sparged bubble columns. AIChE J. 36, 1485–1499. https://doi.org/10.1002/aic.690361004

Qian, D., McLaughlin, J.B., Sankaranarayanan, K., Sundaresan, S., Kontomaris, K., 2006. Simulationof bubble breakup dynamics in homogeneous turbulence. Chem. Eng. Commun. 193, 1038–1063. https://doi.org/10.1080/00986440500354275

Ravelet, F., Colin, C., Risso, F., 2011. On the dynamics and breakup of a bubble rising in a turbulent flow. Cit. Phys. Fluids 23. https://doi.org/10.1063/1.3648035

Renardy, Y., Cristini, V., Li, J., 2002. Drop fragment distributions under shear with inertia. Int. J. Multiph. Flow 28, 1125–1147. https://doi.org/10.1016/S0301-9322(02)00022-8

Renardy, Y.Y., Cristini, V., 2001a. Effect of inertia on drop breakup under shear. Phys. Fluids 13, 7–13. https://doi.org/10.1063/1.1331321

Renardy, Y.Y., Cristini, V., 2001b. Scalings for fragments produced from drop breakup in shear flow with inertia. Phys. Fluids 13, 2161–2164. https://doi.org/10.1063/1.1384469

Richter, T., Keplinger, O., Shevchenko, N., Wondrak, T., Eckert, K., Eckert, S., Odenbach, S., 2018. Single bubble rise in GaInSn in a horizontal magnetic field. Int. J. Multiph. Flow 104, 32–41. https://doi.org/10.1016/J.IJMULTIPHASEFLOW.2018.03.012

Risso, F., Fabre, J., 1998. Oscillations and breakup of a bubble immersed in a turbulent field. J. Fluid Mech. 372, 323–355. https://doi.org/10.1017/S0022112098002705

Saito, Y., Mishima, K., Tobita, Y., Suzuki, T., Matsubayashi, M., Lim, I.C., Cha, J.E., 2005. Application of high frame-rate neutron radiography to liquid-metal two-phase flow research. Nucl. Instruments Methods Phys. Res. A 542, 168–174. https://doi.org/10.1016/j.nima.2005.01.095

Sarma, M., Ščepanskis, M., Jakovičs, A., Thomsen, K., Nikoluškins, R., Vontobel, P., Beinerts, T., Bojarevičs, A., Platacis, E., 2015. Neutron Radiography Visualization of Solid Particles in Stirring Liquid Metal. Phys. Procedia 69, 457–463. https://doi.org/10.1016/J.PHPRO.2015.07.064

Shevchenko, N., Boden, S., Eckert, S., Borin, D., Heinze, M., Odenbach, S., 2013. Application of X-ray radioscopic methods for characterization of two-phase phenomena and solidification processes in

metallic melts. Eur. Phys. J. Spec. Top. 220, 63–77. https://doi.org/10.1140/epjst/e2013-01797-y
Solsvik, J., Jakobsen, H.A., 2015a. Single drop breakup experiments in stirred liquid–liquid tank. Chem. Eng. Sci. 131, 219–234. https://doi.org/10.1016/j.ces.2015.03.059
Solsvik, J., Jakobsen, H.A., 2015b. Single Air Bubble Breakup Experiments in Stirred Water Tank. Int. J. Chem. React. Eng. 13, 477–491. https://doi.org/10.1515/ijcre-2014-0154
Suhas S. Jain, 2017. Flow-induced breakup of drops and bubbles [WWW Document]. URL http://arxiv.org/abs/1701.06157
Takahashi, K., McManamey, W.J., Nienow, A.W., 1992. Bubble size distributions in impeller region in a gas-sparged vessel agitated by a Rushton turbine. J. Chem. Eng. JAPAN 25, 427–432. https://doi.org/10.1252/jcej.25.427
Tao, D., 2005. Role of Bubble Size in Flotation of Coarse and Fine Particles—A Review. Sep. Sci. Technol. 39, 741–760. https://doi.org/10.1081/SS-120028444
Timmel, K., Eckert, S., Gerbeth, G., Stefani, F., Wondrak, T., 2010. Experimental Modeling of the Continuous Casting Process of Steel Using Low Melting Point Metal Alloys - the LIMMCAST Program. ISIJ Int. 50, 1134–1141. https://doi.org/10.2355/isijinternational.50.1134
Timmel, K., Shevchenko, N., Röder, M., Anderhuber, M., Gardin, P., Eckert, S., Gerbeth, G., 2015. Visualization of Liquid Metal Two-phase Flows in a Physical Model of the Continuous Casting Process of Steel. Metall. Mater. Trans. B 46, 700–710. https://doi.org/10.1007/s11663-014-0231-8
Tsouris, C., Tavlarides, L.L., 1994. Breakage and coalescence models for drops in turbulent dispersions. AIChE J. 40, 395–406. https://doi.org/10.1002/aic.690400303
Vejražka, J., Zedníková, M., Stanovský, P., 2017. Experiments on breakup of bubbles in a turbulent flow. AIChE J. 0, 1–18. https://doi.org/10.1002/aic.15935
Vogt, T., Boden, S., Andruszkiewicz, A., Eckert, K., Eckert, S., Gerbeth, G., 2015. Detection of gas entrainment into liquid metals. Nucl. Eng. Des. 294, 16–23. https://doi.org/10.1016/j.nucengdes.2015.07.072
Wang, T., Wang, J., Jin, Y., 2003. A novel theoretical breakup kernel function for bubbles/droplets in a turbulent flow. Chem. Eng. Sci. 58, 4629–4637. https://doi.org/10.1016/j.ces.2003.07.009
Wang, Z., Mukai, K., Izu, D., 1999. Influence of Wettability on the Behavior of Argon Bubbles and Fluid Flow inside the Nozzle and Mold. ISIJ Int. 39, 154–163. https://doi.org/10.2355/isijinternational.39.154
Wang, Z.H., Wang, S.D., Meng, X., Ni, M.J., 2017. UDV measurements of single bubble rising in a liquid metal Galinstan with a transverse magnetic field. Int. J. Multiph. Flow 94, 201–208. https://doi.org/10.1016/j.ijmultiphaseflow.2017.05.001
Xie, Y., Oeters, F., 1994. Measurements of bubble plume behaviour and flow velocity in gas stirred liquid Wood's metal with an eccentric nozzle position. Steel Res. 65, 315–319. https://doi.org/10.1002/srin.199401077
Xie, Y., Orsten, S., Oeters, F., 1992. Behaviour of Bubbles at Gas Blowing into Liquid Wood's Metal. ISIJ Int. 32, 66–75. https://doi.org/10.2355/isijinternational.32.66
Zhang, C., Eckert, S., Gerbeth, G., 2005. Experimental study of single bubble motion in a liquid metal column exposed to a DC magnetic field. Int. J. Multiph. Flow 31, 824–842. https://doi.org/10.1016/j.ijmultiphaseflow.2005.05.001
Zhao, H., Ge, W., 2007. A theoretical bubble breakup model for slurry beds or three-phase fluidized beds under high pressure. Chem. Eng. Sci. 62, 109–115. https://doi.org/10.1016/j.ces.2006.08.008